Available online at www.sciencedirect.com

jmr&t
Journal of Materials Research and Technology

journal homepage: www.elsevier.com/locate/jmrt

Original Article

Multifunctional flexible and stretchable graphite-silicone rubber composites

Agee Susan Kurian [a,*], *Velram Balaji Mohan* [a,b], *Hamid Souri* [a], *Jinsong Leng* [c], *Debes Bhattacharyya* [a,b]

[a] *Centre for Advanced Composite Materials, Faculty of Engineering, The University of Auckland, 314 Khyber Pass Road, Newmarket, Auckland, 1142, New Zealand*
[b] *Plastics Centre of Excellence, Faculty of Engineering, The University of Auckland, 314 Khyber Pass Road, Newmarket, Auckland, 1142, New Zealand*
[c] *Centre for Composite Materials and Structures, Harbin Institute of Technology, HIT Science Park, No. 2 YiKuang Street, Harbin, 150080, PR China*

ARTICLE INFO

Article history:
Received 23 July 2020
Accepted 7 November 2020
Available online 17 November 2020

Keywords:
Graphite
Flexible
Thermal interface devices
Protective circuits
Temperature sensors
Stretchable

ABSTRACT

The demand for stretchable, soft and wearable multifunctional devices based on conductive polymer composites is rapidly growing because of their compelling applications, including physical and physiological measurements on the human body. This paper reports a simple and cost-effective technique to fabricate electrically conductive flexible films with graphite (GRP) flakes and an elastomer, silicone rubber (SR). The mechanical, thermal, electromechanical and electrothermal characterisations of the composites were conducted. While the dynamic electromechanical response of the composites demonstrated their potential applications as wearable sensors, the electrothermal characteristics of the devices showed their suitability to be used as flexible protective circuits and flexible temperature sensors. The synergistic effect of GRP flakes with carbon black (CB) particles was also studied. GRP-SR composites showed a thermal conductivity (TC) of 1.08 W m^{-1} K^{-1} and were thermally stable up to up to 300 °C. The good TC and thermal stability along with their deformability, make them suitable to be used as thermal interface devices in arbitrarily shaped surfaces.

© 2020 The Authors. Published by Elsevier B.V. This is an open access article under the CC BY-NC-ND license (http://creativecommons.org/licenses/by-nc-nd/4.0/).

1. Introduction

Soft and stretchable conductive polymer composites (CPC) have gained widespread attention due to their abilities to be bent, stretched, twisted and compressed reversibly without physical damage. Therefore, these composites can be utilised in various applications such as structural health monitoring [1,2], human motion monitoring [3,4], smart clothing [5,6], and so forth. Diverse fillers have been employed to accomplish CPC such as carbon nanotubes [7,8], graphene [9,10], graphite (GRP) [11,12], carbon black (CB) [13,14], silver [15,16] and gold

* *Corresponding author.*
E-mail address: akur481@aucklanduni.ac.nz (A.S. Kurian).
https://doi.org/10.1016/j.jmrt.2020.11.021
2238-7854/© 2020 The Authors. Published by Elsevier B.V. This is an open access article under the CC BY-NC-ND license (http://creativecommons.org/licenses/by-nc-nd/4.0/).

[17,18]. Among the various fillers, GRP has shown to be a promising candidate over other fillers due to its good electrical conductivity [19], good thermal conductivity [20], biocompatibility [21,22], low percolation threshold owing their high aspect ratio [23], high compressive strength [24], along with their natural abundance [25,26] and low price [27]. To date, GRP has already been used in a wide range of applications namely, electrochemical sensors [28,29], force sensors [29,30], temperature sensors [31], piezoresistive sensors [32], piezoelectric sensors [33] and thermoresistive sensors [34].

When rigid thermal interface materials (TIM) are used, the surface roughness between the two surfaces (the surface of the heat source and the surface of the TIM) can create air-filled gaps preventing the efficient heat transfer as the TC of air is 0.026 W m^{-1} K^{-1} only [35]. Deformable and soft TIM can effectively transfer heat, because they can adhere to even non-planar or curvilinear surfaces and undergo large deformations in a good manner, without creating air gaps [36]. Many studies have been carried out on silicone rubber (SR) based thermally conductive polymer composites (TCPC). However, the reported TC of SR-based composites were small to be used for adequate heat transfer. Graphene/SR composites displayed a TC of 0.30 W m^{-1} K^{-1} [37] while 0.21 W m^{-1} K^{-1} was reported for CNT/SR composites [38], 0.45 W m^{-1} K^{-1} for MWCNT/SR composites [39], 0.55 W m^{-1} K^{-1} for Boron nitride and Aluminium nitride/SR composites [40] and 0.28 W m^{-1} K^{-1} for CNT-BN/SR composites [41]. TCPC was prepared using GRP and SR by melt mixing and solution intercalation, which showed a TC of 0.32 W m^{-1} K^{-1} and 0.24 W m^{-1} K^{-1}, respectively [42]. Krupa et al. fabricated polyethylene/GRP composites by compression moulding, which had a TC of 0.59 W m^{-1} K^{-1} [43]. Hung et al. studied heat conduction in GRP/resin composites, which had a TC of 0.21 W m^{-1} K^{-1} [44]. TC of 400 W m^{-1} K^{-1} for GRP/polymer sheets, 1.59 W m^{-1} K^{-1} for GRP/polyethylene composites, 5.8 W m^{-1} K^{-1} for GRP/epoxy composites and 1.2 W m^{-1} K^{-1} for GRP/polypropylene composites, were reported. However, no reports on the flexibility or the softness of the composites to be used as TIM in curvilinear surfaces or deformable applications [45–48]. Therefore, there is a potential opportunity to develop a multifunctional device that can potentially act as a wearable sensor, flexible temperature sensor, protective circuits, and soft and deformable TIM.

In this work, we have successfully fabricated a novel class of flexible and stretchable TIM that can also function as stretchable large strain sensors, flexible protective circuits and temperature sensors. This was accomplished by taking advantage of a facile, mass-producible fabrication method with low production cost.

2. Materials and methods

2.1. Materials

GRP flakes with size ranging within 50–800 μm and thickness of 1–150 μm were purchased from Sigma–Aldrich, Australia. CB particles with an average diameter of 30 nm were supplied by Orion Engineered Carbons GmbH, Hana, Germany. Toluene was supplied by EPL, New Zealand and two components of Ecoflex® 00–30, platinum catalysed silicones, the SR used in this study, were supplied by Fibreglass, New Zealand as a product of smooth-on, the USA.

2.2. Fabrication of composites

The two components of SR were mixed in an equal volume ratio of 1:1, gently stirred, and then poured into an acrylic mould with dimensions of 20 mm × 90 mm to rest. Finally, the mould was kept for 4 h at room temperature to cure, and a substrate with thickness 1 mm was prepared.

Toluene was added to the fillers GRP and GRP-CB and sonicated for 3 h followed by magnetic stirring for 30 min. Part A of SR was added to the mixture and magnetically stirred for 15 min, followed by the addition of Part B of SR, and the air bubbles were removed using a vacuum chamber. The final mixture was gently poured into an Acrylic mould and left for 4 h at room temperature. The top layer was prepared by casting the SR solution. The final sandwich structured composite was cured in an oven at 80 °C for 2 h, followed by 1 h at 100 °C. After curing, the composites were detached from the mould. Mixtures of GRP-SR in toluene were prepared with 10.26 wt.% of GRP. GRP-CB-SR mixtures were prepared with 0.64 wt.%, 1.27 wt.% 1.89 wt.% of CB.

Composite samples for the characterisations from Section 3.3 were prepared by dispersing GRP in SR using magnetic stirring. GRP-CB-SR composites were prepared by adding CB into the SR and magnetically stirred for 10 min, and then GRP flakes were added and magnetically stirred for 10 min. It was then transferred into an Acrylic mould with dimensions of 20 mm × 90 mm.

2.3. Characterisation

The DC Current–Voltage (I–V) characteristics were measured by Keithley 2100 digital multimeter (DMM). Dynamic cyclic stretch-release testings were monitored by Keithley 2612, Keithley Instruments. Temperature-dependent resistance characteristics were studied with Keithley 2100 DMM. Morphological studies on the composites and conductive particles were carried out via microscopy images using a Leica DFC 290 and scanning electron microscopy by a Hitachi SU-70. To understand the electromechanical response of the composites, the structural changes appearing at different levels of stretching and releasing were observed. The sandwich structured composites encapsulated within SR layers were inflexibly fixed by two Acrylic grips. With an automated motion control stage and a four-point conductivity meter (Keithley 2612), the output voltage drop across a specified length during extension and relaxation cycles were measured. Multiples cycles of stretching and relaxation were conducted to study the performance of the composite as a stretchable sensor.

Mechanical testing of the composites was carried out following ASTM D-412 using Instron 5567, universal testing machine and the samples were prepared in dog bone shape in accordance with the standard. The Nicolet iS50 FTIR spectrometer was used with a diamond attenuated total reflectance (ATR) element to record vibrational spectra. The spectra were obtained in the range of 4000-400 cm^{-1} and averaged

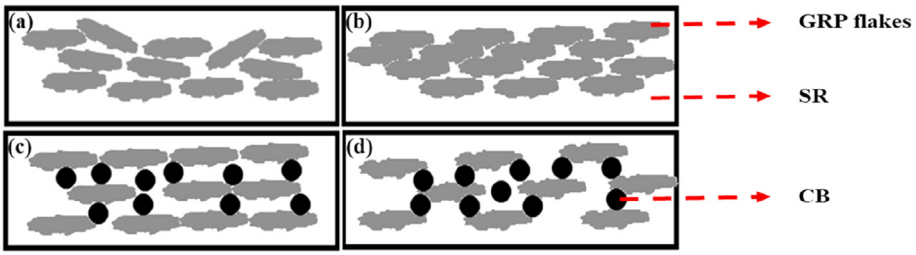

Fig. 1 – Schematic view of the conductive networks in GRP-SR composite sensors (a) at zero strain (b) when stretched, GRP-CB-SR composites (c) at zero strain, and (d) when stretched.

over 32 scans. Omnic® ESP, version 7.1, was used for data acquisition and analysis. The crystallisation and melting characteristics of the composites were studied by differential scanning calorimetry (DSC) using a DSC Q1000 analyser in a nitrogen atmosphere with a flow rate of 50 mL/min. Dynamic mechanical thermal analysis (DMTA) was conducted on a TA instrument Q5000 series in a nitrogen atmosphere. The thermal stability of the composites was examined using Q-800 series. For this, samples of approximately 10 mg were heated from 30 °C to 700 °C in a nitrogen atmosphere with a heating rate of 10 °C/min, and the sample weight was monitored with the increase in temperature. The TC was measured with TC-30, Mathis, TC instrument. Raman analysis was carried out using Renishaw RM 1000 Raman Microprobe with an air-cooled argon-ion 488 nm excitation laser. The nano-mechanical studies were conducted by Environmental Atomic Force Microscope cypher ES (Asylum Research, Oxford Instruments).

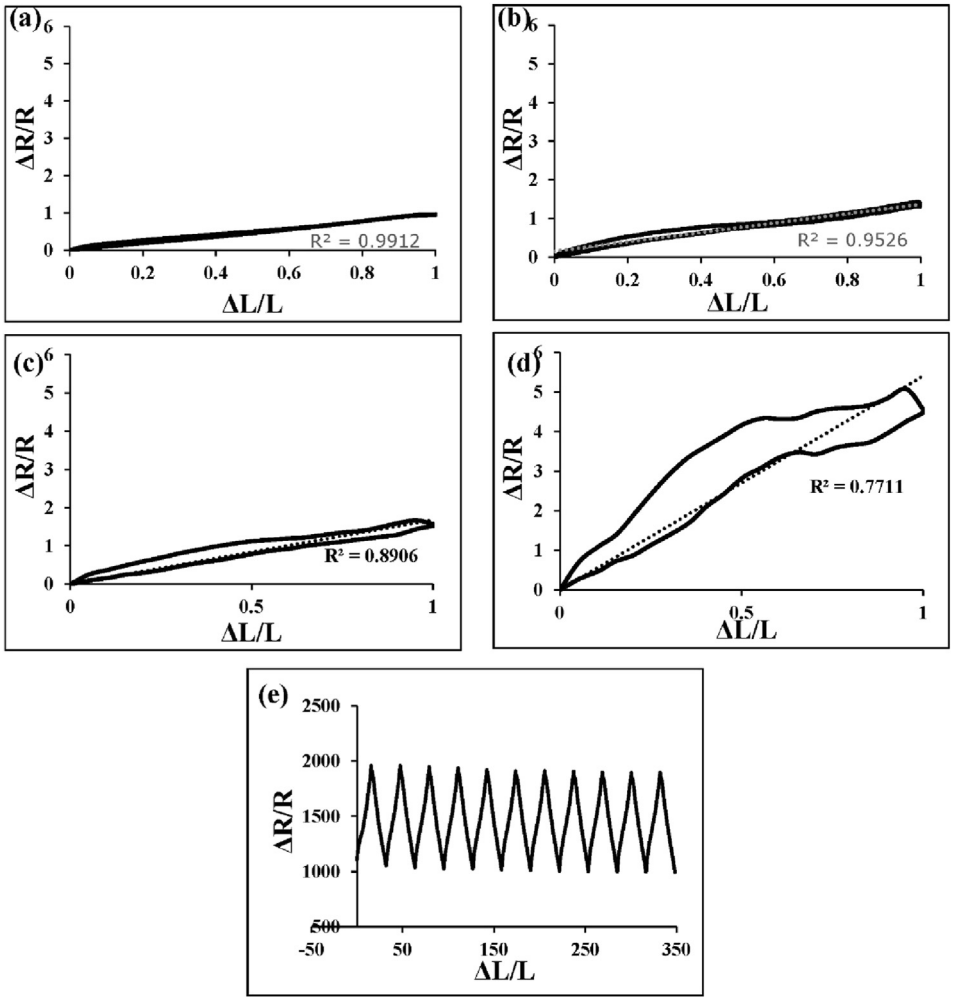

Fig. 2 – Electromechanical characteristics of (a) GRP-SR composite sensor, and GRP-CB-SR composite sensor with varying wt.% of CB (b) 0.64 wt.%, (c) 1.27 wt.%, and (d) 1.89 wt.%, and (e) durability test result of GRP-SR composite sensor.

3. Results and discussion

3.1. *Electromechanical characteristics of the GRP-SR composites*

When the GRP-SR composite sensor is stretched, the resistance is increased due to the rearrangement of the GRP in the conductive networks. Fig. 1(a) and (b) show the schematics of the filler arrangement within the SR matrix before and after relaxation. Unlike previously reported GNP-SR film [49], the surface of the as-prepared film is not uniform, as demonstrated in Fig. 3(d) and Fig. S1(a), which might be due to the large particle size of the GRP flakes. Similar to GNP-SR strain sensors and CB-SR strain sensors, GRP-SR strain sensors also exhibited a positive piezoresistance [49]. The low viscosity of the SR [50] facilitates a good connection between the flakes. When GRP-SR film is stretched, owing to the difference in Young's modulus of the SR and the GRP, the SR elastomeric chains are strained, allowing the GRP flakes to slip one top of each other, resulting in a variation in their contact surface area. However, GRP flakes can hardly slide on each other, mainly due to the higher surface roughness of GRP, as shown in Fig. 3(b) and (c). Consequently, the resistance did not change as large as the case of GNP [49]. Upon release, the resistance marginally dropped because the surface roughness of the GRP flakes prevents the restacking of the GRP flakes.

As in Fig. 1(a), dispersing GRP in a solvent and casting film helps the GRP flakes to overlay on each other. Nevertheless, there is only minor contact between the surfaces due to the rough surface of the GRP. We have observed that GRP-SR composites with 4.10 wt.% were non-conductive while GRP-SR composites with 5.41 wt.% were conductive. Previous studies reported on the synergistic effect of hybrid fillers, and hence CB was added to the GRP-SR composites to study the variations in the conductivity of the composites [51–53]. The spherically shaped CB particles can bridge the gaps between the GRP sheets and favour electron movement, and hence, the conductivity increases. The introduction of CB particles was found to have a remarkable effect on the electromechanical characteristics of the GRP-SR composite sensor. Fig. 1(c) and (d) show the schematics of the GRP-CB-SR composites. CB

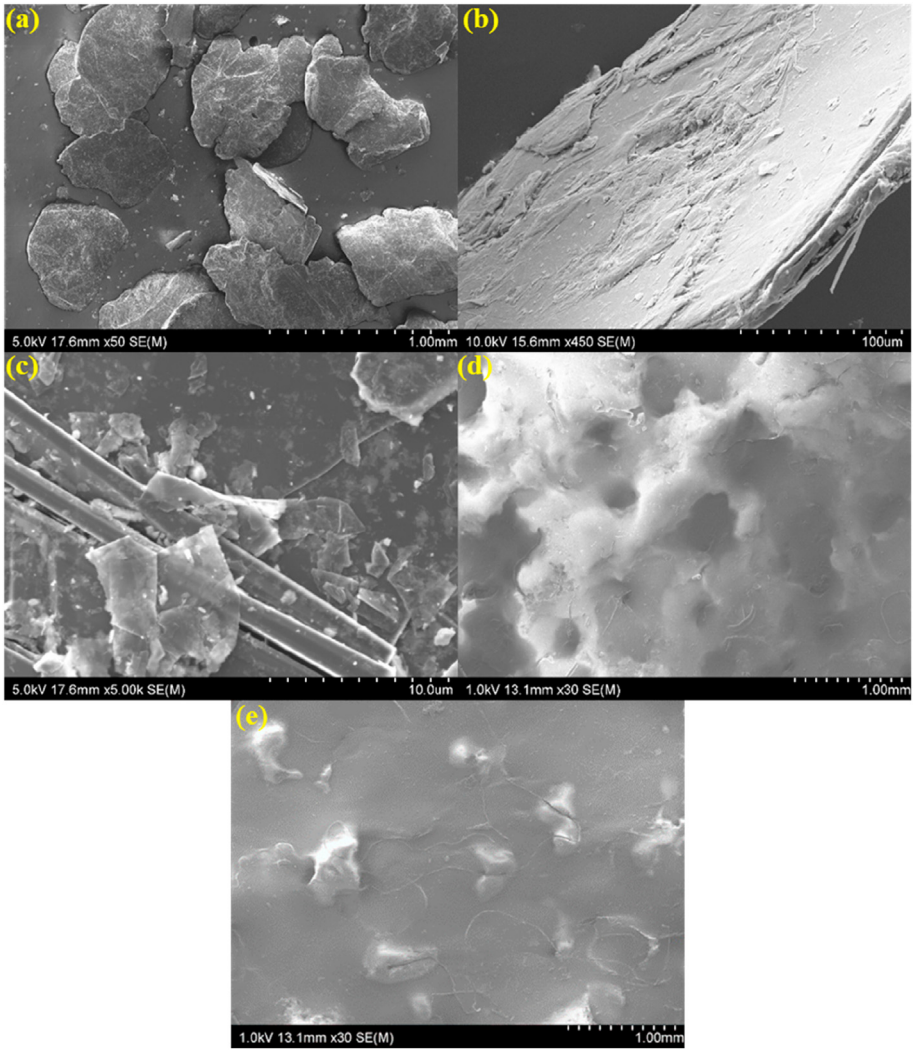

Fig. 3 – SEM images (a) GRP flakes, (b) a single GRP flake at higher magnification, (c) single GRP surface indicating roughness, (d) the surface of as-prepared GRP-SR sensor, and (e) the surface of GRP-SR sensor under stretching.

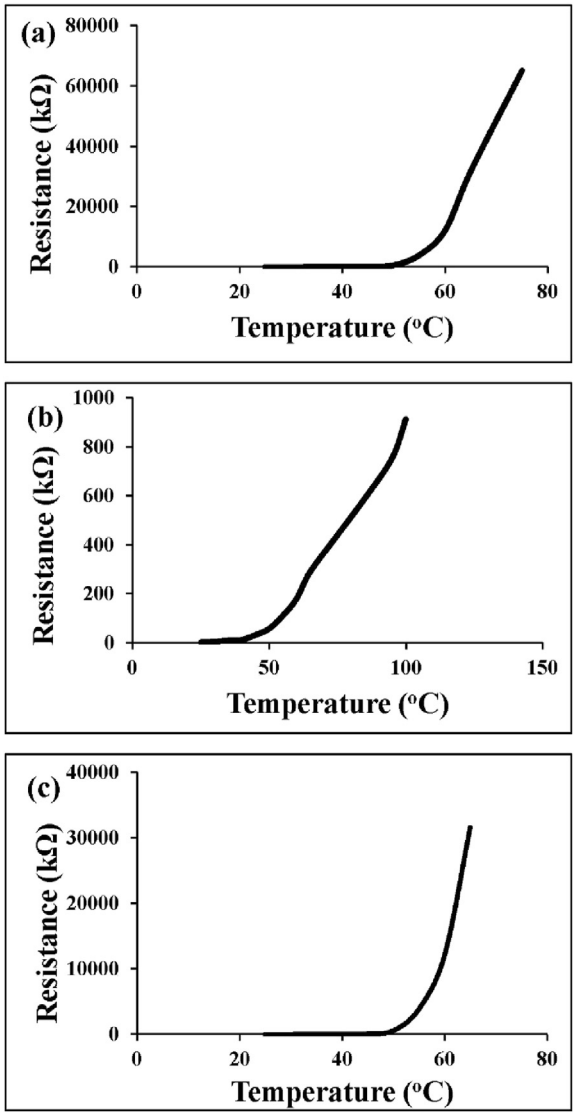

Fig. 4 – R–T characteristics of GRP-SR composite film of 2.5 cm length with (a) 9.76 wt.% of GRP (b) 10.81 wt.% of GRP, and (c) 9.09 wt.% of GRP.

particles stay on the edge planes of the GRP flakes and bridge the gap between the GRP, thereby increasing the conductive networks in the matrix. Fig. 2(a) displays the variations in resistance of the GRP-SR composite sensor with regards to strain. The piezoresistive characteristics showed excellent linearity with low hysteresis. GRP-SR strain sensor always traversed a low resistance path during relaxation similar to previously reported GNP-SR strain sensors, but with a lower hysteresis [49]. When stretched, CB particles act as a ball bearing, facilitating to move the GRP flakes more effortlessly than in the absence of CB. CB particles, which rolls along with the polymer chains, allowing GRP to move apart more distance than in the absence of CB, as in Fig. 2(b). During relaxation also, CB particles roll back, generating more conductive networks which cause a resistance drop. However, when CB loading is increased, the hysteresis and non-linearity of the curves increases, as exhibited in Fig. 2(c) and (d). It could be due to the agglomerations of the CB particles which hinder the GRP movement. Hence, it can be concluded that higher CB loading obstructs the filler movement on stretching and relaxation. Fig. S2 displays the change in resistance with CB wt.% which clearly shows an increase in conductivity with increasing CB loading. Fig. 2(e) demonstrates the durability of the sensor under multiple cycles of stretching and relaxation. The sensor has a stable electromechanical characteristic suitable to be used as large strain sensing applications.

Fig. 3(a) shows the SEM images of GRP flakes while the SEM images of a single GRP flake (Fig. 3(b) and (c)) demonstrating its rough surface. The surface roughness of GRP has a significant effect on the piezoresistive properties of GRP-SR composites. Fig. S1 presents the optical images of the changes in the surface of the film during stretching and releasing. Fig. S1(a) demonstrates the strain sensor at zero strain and Fig. S1(b) displays the sensor under 50% of strain. It is apparent that the surface of the film becomes more uniform as the GRP align themselves in the direction of applied strain. Fig. S1(c) depicts the film under 100% strain, where more alignment of GRP flakes was observed. Fig. S1(d) represents the film under 50% relaxation while Fig. S1(e) demonstrates the film when recovered to zero strain. In contrast to GNP-SR [49] composite sensors, no crests and troughs were observed.

3.2. *R-T characteristics of GRP-SR composites*

The study of the temperature-dependent resistance characteristics of the fabricated strain sensor helps us to understand the conductivity mechanism of the composites and to find a model for the temperature compensation of resistance for real-time applications. Similar to GNP-SR sensors [49], the resistance showed an increasing tendency with an increase in temperature, displaying a positive temperature coefficient (PTC) of resistance. Owing to the high conductivity of GRP flakes, it can be concluded that the voltage drops across the graphite flakes are trivial when compared to the voltage drop across the polymer phase. GRP-polymer shows PTC on heating [11,54,55] due to the semi-metallic nature of graphite [56] and the expansion of the polymer layer between the fillers, which occurs on heating. The thermal expansion of the polymer decreases the contact between the adjacent GRP flakes resulting in increased resistance. Fig. 4(a) represents the variations in resistance of GRP-SR composite film with GRP 9.76 wt.%. GRP-SR composite with 10.26 wt.% of GRP showed less change in resistance while GRP-SR composite with

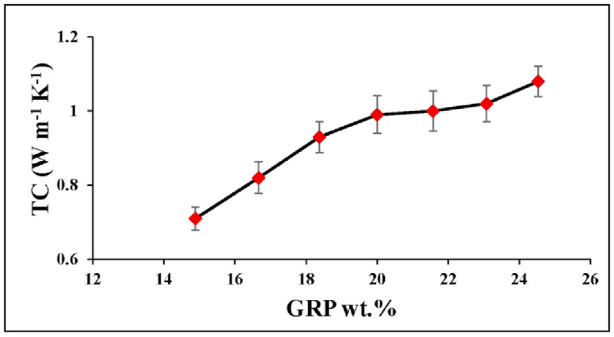

Fig. 5 – TC of GRP-SR composites with varying GRP wt.%.

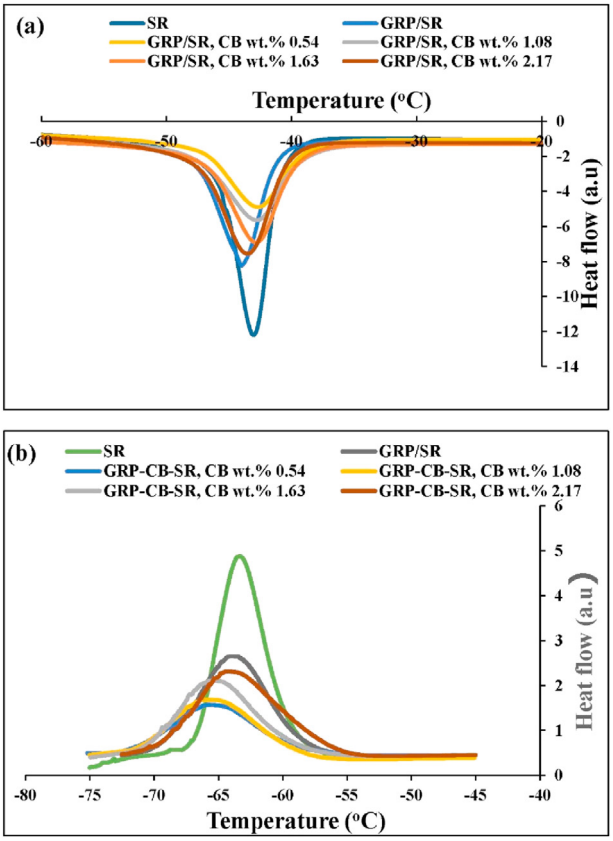

Fig. 6 – DSC curves of SR and filled SR composites (a) melting (b) crystallisation.

9.09 wt.% of GRP showed more change in resistance and became non-conductive (above 100 MΩ) at about 65 °C, Fig. 4(c). This proposes that the change in resistance with temperature depends on the expansion of the polymer layer between the flakes which hinders the motion of the electrons between the neighbouring GRP flakes. The polymer expansion reduced the number of conductive networks, and hence the resistance increased. This distinctive behaviour makes them suitable to be utilised as flexible protective circuits in which the composite can deactivate the circuit upon fault condition when the temperature rises above a certain limit. The change in resistance values of the composites having less GRP content is more which suggests that polymer expansion plays a pivotal role in resistance change upon heating. Fig. S3 depicts the application of GRP-SR sensor as a flexible circuit breaker. Fig. S3(a) illustrates the GRP-SR sensor at room temperature while Fig. S3(b), S3(c) and S3(d) show the GRP-SR sensor at higher tempratures. In Fig. S3(a), the sensor conducts electricity and the light emitting diode (LED) glows. In the following figures, it can be seen that the intensity of the LED decreases due to the increase in resistance (Fig. S3(b) and S3(c)). The sensor conducts electricity when the temperature is at 69 °C and as a result, the LED lights, and finally at 71 °C, the sensor does not conduct electricity and the light of the LED turns off, Fig. S3(d). The variations in resistance with the temperature of GRP-SR composites with 10.81 wt.% of GRP increased with temperature displaying a PTC of resistance, as depicted in Fig. 4(b). They remained conductive up to 100 °C, which makes them appropriate to be used as flexible temperature sensors.

3.3. *Thermal conductivity of GRP-SR composites*

GRP-SR composites with 24.53 wt.% of GRP demonstrated the highest TC of 1.08 W m^{-1} K^{-1}. The TC decreased by lowering GRP loadings, as illustrated in Fig. 5. TC of the hybrid filler system is listed in Table-S1. The TC of 13.04 wt.% of GRP-SR composite is 0.66 (W m^{-1} K^{-1}), while the inclusion of 0.54 wt.% of CB marginally increased the TC. TC increased further with a higher CB loading of 1.08 wt.%. However, TC decreased with a further addition of CB loading, which might be due to the agglomerations of CB particles, obstructing to

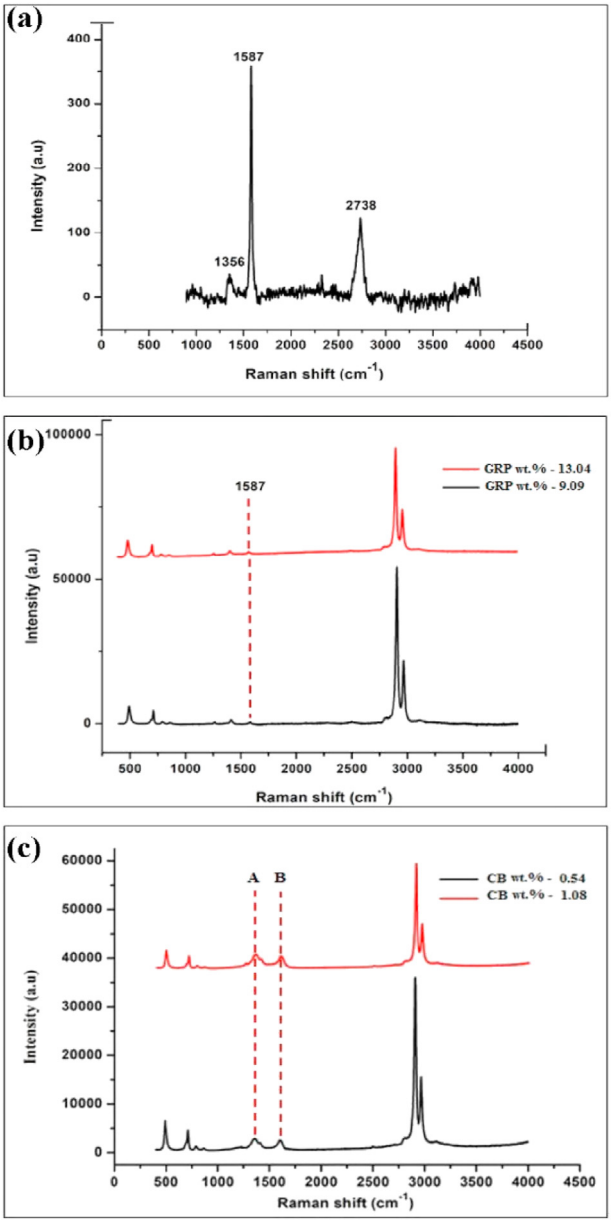

Fig. 7 – Raman spectrum of GRP-SR composites (a) GRP flakes, (b) GRP-SR composites, and (c) GRP-CB-SR composites.

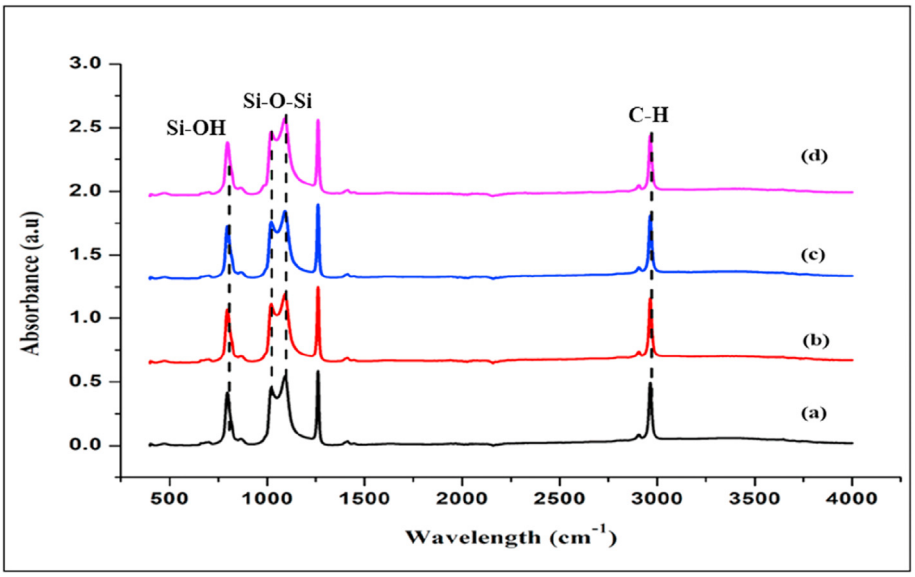

Fig. 8 – FTIR spectra of (a) SR (b) GRP-SR composites with GRP wt.% 13.04 (c) GRP-CB-SR composites with GRP wt.% 12.97 CB wt.% 0.54, and (d) GRP-CB-SR composites with GRP wt.% 12.83 CB wt.% 1.60.

the phonon transmission through the composite. The good TC and the stretchability, as well as the flexibility of GRP-SR composites, make them applicable as thermal interface devices in various advanced applications. Fig. S4(a), (b) and (c) demonstrate the good stretchability and flexibility of the GRP-SR film and Fig. S4 (d) shows the sensor fabricated for wearable applications. The softness along with their deformability of the GRP-SR film allows them to make the surfaces of heat source fully in contact without airgaps which makes them suitable to be used as deformable TIM.

3.4. *DSC analysis of the composites*

The DSC melting curves of pristine SR and SR filled with GRP and CB composites are shown in Fig. 6. When GRP is added to SR, T_m is shifted to a lower temperature side (Fig. 6(a)). Here, the GRP acts as a physical barrier hindering the melting. However, it is observed that the addition of CB slightly favoured melting temperature, leading to an increase in T_m [57,58]. Increase of T_m implies that the higher energy is required to disrupt the crystal lattice. However, it is perceived that though a small amount of CB promotes nucleation, higher loading has lowered the T_m [59]. Fig. 6(b) exhibits the DSC crystallisation curves of the composites. The T_c of the filled SR composites was shifted to the lower temperature side, indicating that the fillers did not improve crystallisation [60].

3.5. *Thermogravimetric analysis (TGA)*

Many applications require CPC with good thermal stability such as fuel cells, batteries and heat exchangers [61]. Thus, the thermal stability of the GRP-SR composites was analysed via TGA. Fig. S5 presents the weight versus temperature profile of neat SR and GRP-SR composites. It was observed that prominent weight loss took place above around 300 °C, which is the decomposition temperature of SR. The results reveal that weight loss mainly occurred in the range 300–600 °C with the negligible change above 600 °C. An introduction of GRP into the SR decreased the thermal stability. The addition of CB between 0.54 wt.% and 1.08 wt.% improved the thermal stability. However, the inclusion of the CB above 1.08 wt.% slightly decreased thermal stability, which might be due to the existence of the agglomerations at higher CB loadings. Based on these results, it may be concluded that the thermal stability and decomposition temperature of the GNP-SR composites improved with the presence of CB between 0.54 wt.% and 1.08 wt.%.

3.6. *Raman spectroscopy*

The chemical interactions between the various components in the matrix were studied using Raman spectroscopy [62,63]. Fig. 7(a) portrays the characteristics Raman bands of GRP; D at 1356 cm^{-1}, G at 1587 cm^{-1} and 2D at 2738 cm^{-1} [64,65]. The narrow peak and position of G peak confirm that the GRP used in this study had high purity. Fig. 7(b) displays the Raman bands of GRP-SR composites at two different SR concentrations. Both curves indicate the presence of GRP at wavelength 1587 cm^{-1} which shows the absence of any chemical modifications. Fig. 7(c) exhibits the Raman bands of GRP-CB-SR composites at two different loadings of CB wt.%. A and B shows the D band and G band of CB, respectively. Fig. 7(b) and 7(c) reveal that the inclusion of GRP and CB did not make any changes in the peak positions, which suggests that the fillers could not make any chemical modifications.

3.7. *FTIR analyses*

Fig. 8 shows the FTIR spectra of the SR and the filled SR composites. It is apparent from the spectra that the inclusion GRP flakes has not created any new peaks or any changes in

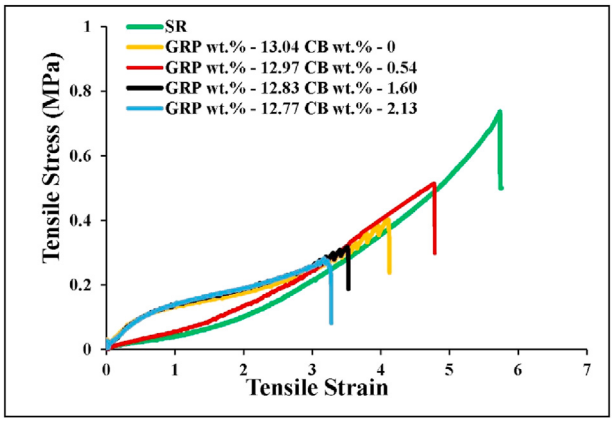

Fig. 9 – Mechanical properties of the composites.

the peak positions. Hence, it may be concluded that the fillers could not chemically modify the composites.

3.8. *Mechanical properties*

Fig. 9 shows the results of the mechanical tests performed, demonstrating the effects of incorporating the GRP and CB in SR. It manifests that the incorporation of GRP improved tensile strength. It is observed that the inclusion of a small amount CB into the GRP-SR composites, modified the mechanical properties. Among the filled composites examined, the GRP-SR composites with 0.54 wt.% of CB displayed the highest elongation at break. Further addition of CB improved the tensile strength at the expense of elongation at break, as presented in Fig. 9. However, the curves of GRP-SR, GRP-CB-SR with 1.60 wt.% of CB and 2.13 wt.% of CB are not smooth. It reveals that when the GRP-SR film is stretched, the rough surface of GRP prevents the free movement of GRP within the elastomeric matrix, as schematised in Fig. 1(b). However, the addition of a small amount of CB favours the movement of GRP in the polymer matrix while the inclusion of more CB hampers the filler movement.

4. Conclusions

We have developed deformable GRP-SR composites using simple and low-cost procedures. The mechanical, thermal, electromechanical, electrothermal, and optical characteristics of the composites were investigated. The influence of the addition of a second filler, CB particles, on these properties has also been studied, and it is concluded that the inclusion of CB could alter the thermal and mechanical properties of GRP-SR composites. The good TC of soft, flexible and stretchable GRP-SR composites makes them suitable to be used as TIM in many sophisticated applications such as stretchable heaters, stretchable conductors and many more. Moreover, the electrothermal characteristics of the GRP-SR composites displayed a PTC, and they can be utilised as flexible protective circuits and temperature sensors. The good dynamic electromechanical characteristics and mechanical compliance revealed their feasibility to be employed as large strain wearable sensors.

Declaration of Competing Interest

The authors declare no conflict of interests.

Acknowledgements

This work was supported by the Ministry of Business, Innovation and Employment, New Zealand (Grant No: 3706657). The authors are grateful to the CACM technicians for their technical support.

Appendix A. Supplementary data

Supplementary data to this article can be found online at https://doi.org/10.1016/j.jmrt.2020.11.021.

REFERENCES

[1] Alexopoulos N, Bartholome C, Poulin P, Marioli-Riga Z. Structural health monitoring of glass fiber reinforced composites using embedded carbon nanotube (CNT) fibers. Compos Sci Technol 2010;70:260–71.
[2] Lammering R, Gabbert U, Sinapius M, Schuster T, Wierach P. Lamb-wave based structural health monitoring in polymer composites. Springer; 2017.
[3] Souri H, Bhattacharyya D. Highly sensitive, stretchable and wearable strain sensors using fragmented conductive cotton fabric. J Mater Chem C 2018;6:10524–31.
[4] Souri H, Bhattacharyya D. Highly stretchable multifunctional wearable devices based on conductive cotton and wool fabrics. ACS Appl Mater Interfaces 2018;10:20845–53.
[5] Huang GW, Xiao HM, Fu SY. Wearable electronics of silver-nanowire/poly (dimethylsiloxane) nanocomposite for smart clothing. Sci Rep 2015;5:13971.
[6] Singh AV, Rahman A, Kumar NS, Aditi A, Galluzzi M, Bovio S, et al. Bio-inspired approaches to design smart fabrics. Mater Des 2012;36:829–39. 1980-2015.
[7] Yamada T, Hayamizu Y, Yamamoto Y, Yomogida Y, Izadi-Najafabadi A, Futaba DN, et al. A stretchable carbon nanotube strain sensor for human-motion detection. Nat Nanotechnol 2011;6:296.
[8] Kurian AS, Giffney T, Lee J, Travas-Sejdic J, Aw KC. Printing of CNT/silicone rubber for a wearable flexible stretch sensor. In: SPIE smart materials and structures, organiser. Proceedings volume 9798 electroactive polymer actuators and devices (EAPAD) 2016 mar 20-24; 2016. 97980K. Las Vegas,Nevada, United States.
[9] Mohan VB, Krebs BJ, Bhattacharyya D. Development of novel highly conductive 3D printable hybrid polymer-graphene composites. Mater Today Commun 2018;17:554–61.
[10] Tarhini A, Tehrani-Bagha A. Graphene-based polymer composite films with enhanced mechanical properties and ultra-high in-plane thermal conductivity. Compos Sci Technol 2019;184:107797.
[11] Bessonov A, Kirikova M, Haque S, Gartseev I, Bailey MJ. Highly reproducible printable graphite strain gauges for flexible devices. Sensor Actuator Phys 2014;206:75–80.
[12] Tadakaluru S, Thongsuwan W, Singjai P. Stretchable and flexible high-strain sensors made using carbon nanotubes

and graphite films on natural rubber. Sensors 2014;14:868–76.
[13] Kong JH, Jang NS, Kim SH, Kim JM. Simple and rapid micropatterning of conductive carbon composites and its application to elastic strain sensors. Carbon 2014;77:199–207.
[14] Ventrelli L, Beccai L, Mattoli V, Menciassi A, Dario P. Development of a stretchable skin-like tactile sensor based on polymeric composites. In: 2009 IEEE international conference on robotics and biomimetics (ROBIO). IEEE; 2009. p. 123–8.
[15] Cheng Y, Wang R, Sun J, Gao L. Highly conductive and ultrastretchable electric circuits from covered yarns and silver nanowires. ACS Nano 2015;9:3887–95.
[16] Houghton T, Vanjaria J, Yu H. Conductive and stretchable silver-polymer blend for electronic applications. In: 2016 IEEE 66th electronic components and technology conference (ECTC). IEEE; 2016. p. 812–6.
[17] Gong S, Schwalb W, Wang Y, Chen Y, Tang Y, Si J, et al. A wearable and highly sensitive pressure sensor with ultrathin gold nanowires. Nat Commun 2014;5:3132.
[18] Murphy CJ, Orendorff CJ. Alignment of gold nanorods in polymer composites and on polymer surfaces. Adv Mater 2005;17:2173–7.
[19] Glover P. Graphite and electrical conductivity in the lower continental crust: a review. Phys Chem Earth 1996;21:279–87.
[20] Liu Z, Guo Q, Shi J, Zhai G, Liu L. Graphite blocks with high thermal conductivity derived from natural graphite flake. Carbon 2008;46:414–21.
[21] Mücksch C, Urbassek HM. Molecular dynamics simulation of free and forced BSA adsorption on a hydrophobic graphite surface. Langmuir 2011;27:12938–43.
[22] Zolkin P. Study of graphite materials to be used in medicine. Int Polym Sci Technol 2005;32:67–8.
[23] Chen L, Chen G, Lu L. Piezoresistive behavior study on finger-sensing silicone rubber/graphite nanosheet nanocomposites. Adv Funct Mater 2007;17:898–904.
[24] Kim JH, Lee YS. Characteristics of a high compressive strength graphite foam prepared from pitches using a PVA–AAc solution. J Ind Eng Chem 2015;30:127–33.
[25] Chen G, Wu C, Weng W, Wu D, Yan W. Preparation of polystyrene/graphite nanosheet composite. Polymer 2003;44:1781–4.
[26] Chen G, Weng W, Wu D, Wu C. PMMA/graphite nanosheets composite and its conducting properties. Eur Polym J 2003;39:2329–35.
[27] Kawde AN, Baig N, Sajid M. Graphite pencil electrodes as electrochemical sensors for environmental analysis: a review of features, developments, and applications. RSC Adv 2016;6:91325–40.
[28] Purushothama H, Nayaka YA, Vinay M, Manjunatha P, Yathisha R, Basavarajappa K. Pencil graphite electrode as an electrochemical sensor for the voltammetric determination of chlorpromazine. J Sci: Advanced MaterDev 2018;3:161–6.
[29] Monteiro MK, Paiva SS, da Silva DR, Vilar VJ, Martínez-Huitle CA, dos Santos EV. Novel cork-graphite electrochemical sensor for voltammetric determination of caffeine. J Electroanal Chem 2019;839:283–9.
[30] Nag A, Feng S, Mukhopadhyay S, Kosel J, Inglis D. 3D printed mould-based graphite/PDMS sensor for low-force applications. Sensors and Actuators A: Physical. 2018;280:525–34.
[31] Shih WP, Tsao LC, Lee CW, Cheng MY, Chang C, Yang YJ, et al. Flexible temperature sensor array based on a graphite-polydimethylsiloxane composite. Sensors 2010;10:3597–610.
[32] Ren TL, Tian H, Xie D, Yang Y. Flexible graphite-on-paper piezoresistive sensors. Sensors 2012;12:6685–94.
[33] Mall S, Coleman J. Monotonic and fatigue loading behavior of quasi-isotropic graphite/epoxy laminate embedded with piezoelectric sensor. Smart Mater Struct 1998;7:822.
[34] Dinh T, Phan HP, Dao DV, Woodfield P, Qamar A, Nguyen NT. Graphite on paper as material for sensitive thermoresistive sensors. J Mater Chem C 2015;3:8776–9.
[35] Gwinn JP, Webb RL. Performance and testing of thermal interface materials. Microelectron J 2003;34:215–22.
[36] Bartlett MD, Kazem N, Powell-Palm MJ, Huang X, Sun W, Malen JA, et al. High thermal conductivity in soft elastomers with elongated liquid metal inclusions. Proc Natl Acad Sci Unit States Am 2017;114:2143–8.
[37] Tian L, Wang Y, Li Z, Mei H, Shang Y. The thermal conductivity-dependant drag reduction mechanism of water droplets controlled by graphene/silicone rubber composites. Exp Therm Fluid Sci 2017;85:363–9.
[38] Li ZW. Thermoelectric properties of carbon nanotube/silicone rubber composites. J Exp Nanosci 2017;12:188–96.
[39] Katihabwa A, Wang W, Jiang Y, Zhao X, Lu Y, Zhang L. Multi-walled carbon nanotubes/silicone rubber nanocomposites prepared by high shear mechanical mixing. J Reinforc Plast Compos 2011;30:1007–14.
[40] Ou Z, Gao F, Zhao H, Dang S, Zhu L. Research on the thermal conductivity and dielectric properties of AlN and BN co-filled addition-cure liquid silicone rubber composites. RSC Adv 2019;9:28851–6.
[41] Xue Y, Li X, Wang H, Zhang D, Chen Y. Thermal conductivity improvement in electrically insulating silicone rubber composites by the construction of hybrid three-dimensional filler networks with boron nitride and carbon nanotubes. J Appl Polym Sci 2019;136:46929.
[42] Mu Q, Feng S. Thermal conductivity of graphite/silicone rubber prepared by solution intercalation. Thermochim Acta 2007;462:70–5.
[43] Krupa I, Novák I, Chodák I. Electrically and thermally conductive polyethylene/graphite composites and their mechanical properties. Synth Met 2004;145:245–52.
[44] Hung MT, Choi O, Ju YS, Hahn H. Heat conduction in graphite-nanoplatelet-reinforced polymer nanocomposites. Appl Phys Lett 2006;89:023117.
[45] Zhou S, Xu J, Yang QH, Chiang S, Li B, Du H, et al. Experiments and modeling of thermal conductivity of flake graphite/polymer composites affected by adding carbon-based nano-fillers. Carbon 2013;57:452–9.
[46] Ye CM, Shentu BQ, Weng ZX. Thermal conductivity of high density polyethylene filled with graphite. J Appl Polym Sci 2006;101:3806–10.
[47] Ganguli S, Roy AK, Anderson DP. Improved thermal conductivity for chemically functionalized exfoliated graphite/epoxy composites. Carbon 2008;46:806–17.
[48] Kalaitzidou K, Fukushima H, Drzal LT. Multifunctional polypropylene composites produced by incorporation of exfoliated graphite nanoplatelets. Carbon 2007;45:1446–52.
[49] Kurian AS, Mohan VB, Bhattacharyya D. Embedded large strain sensors with graphene-carbon black-silicone rubber composites. Sens Actuators A: Phys 2018;282:206–14.
[50] Smooth-On, Ecoflex Series Product Overview, https://www.sculpt.com/2017/Tech/MsdsTechSheets/TechSheets/TECH_SHEET_Ecoflex.pdf
[51] Xie P, Zhang Z, Wang Z, Sun K, Fan R. Targeted double negative properties in silver/silica random metamaterials by precise control of microstructures. Research 2019;2019:1021368.
[52] Fan G, Zhao Y, Xin J, Zhang Z, Xie P, Cheng C, et al. Negative permittivity in titanium nitride-alumina composite for

functionalized structural ceramics. J Am Ceram Soc 2020;103:403–11.
[53] Wang L, Song P, Lin CT, Kong J, Gu J. 3D shapeable, superior electrically conductive cellulose nanofibers/Ti3C2Tx MXene aerogels/epoxy nanocomposites for promising EMI shielding. Research 2020:2020.
[54] Takahashi K, Hahn HT. Investigation of temperature dependency of electrical resistance changes for structural management of graphite/polymer composite. J Compos Mater 2011;45:2603–11.
[55] Roberts DE, VI. The effect of temperature and magnetization on the resistance of graphite. The London, Edinburgh, and Dublin Philosophical Magazine and Journal of Science 1913;26:158–76.
[56] Chernozatonskii LA, Sorokin PB, Belova E, Brüning J, Fedorov AS. Metal-semiconductor (semimetal) superlattices on a graphite sheet with vacancies. JETP Lett (Engl Transl) 2006;84:115–8.
[57] Ajorloo M, Fasihi M, Ohshima M, Taki K. How are the thermal properties of polypropylene/graphene nanoplatelet composites affected by polymer chain configuration and size of nanofiller? Mater Des 2019;181:108068.
[58] Sreekanth M, Bambole V, Mhaske S, Mahanwar P. Effect of particle size and concentration of flyash on properties of polyester thermoplastic elastomer composites. J Miner Mater Char Eng 2009;8:237.
[59] Wang Y, Cheng L, Cui X, Guo W. Crystallization behavior and properties of glass fiber reinforced polypropylene composites. Polymers 2019;11:1198.
[60] Othman N, Ismail H, Mariatti M. Effect of compatibilisers on mechanical and thermal properties of bentonite filled polypropylene composites. Polym Degrad Stabil 2006;91:1761–74.
[61] Santamaria A, Zhang J. Metal foam microchannel heat exchangers for cooling of fuel cells and flow batteries. In: ASME 2017 fluids engineering division summer meeting. American Society of Mechanical Engineers Digital Collection; 2017.
[62] Fan G, Jiang Y, Xin J, Zhang Z, Fu X, Xie P, et al. Facile synthesis of Fe@ Fe3C/C nanocomposites derived from bulrush for excellent electromagnetic wave-absorbing properties. ACS Sustainable Chem Eng 2019;7:18765–74.
[63] Fan G, Jiang Y, Hou C, Deng X, Liu Z, Zhang L, et al. Extremely facile and green synthesis of magnetic carbon composites drawn from natural bulrush for electromagnetic wave absorbing. J Alloys Compd 2020:155345.
[64] Guerra V, Wan C, Degirmenci V, Sloan J, Presvytis D, Watson M, et al. Characterisation of graphite nanoplatelets (GNP) prepared at scale by high-pressure homogenisation. J Mater Chem C 2019;7:6383–90.
[65] Nagashima K, Nara M, Matsuda Ji. Raman spectroscopic study of diamond and graphite in ureilites and the origin of diamonds. Meteoritics Planet Sci 2012;47:1728–37.